Eur. Phys. J. E (2014) **37**: 51
DOI 10.1140/epje/i2014-14051-0

THE EUROPEAN PHYSICAL JOURNAL E

Regular Article

Worm-like micelles in water solutions of 1, 4 poly (1, 3-butadiene)-polyethylene oxide diblock copolymer

Brisa Arenas-Gómez[1,2], Marko Vinceković[1], Cristina Garza[1], and Rolando Castillo[1,a]

[1] Instituto de Física, Universidad Nacional Autónoma de México, P. O. Box 20-264, México, D. F., 01000, México
[2] Departamento de Física, Centro de Investigación y de Estudios Avanzados del IPN, P. O. Box 14-740, México, D. F., 07000, México

Received 21 May 2014
Published online: 26 June 2014 –

Abstract. The main purpose of this study is to determine for the first time the structure of the self-assembled aggregates in the system made of 1,4 poly(1,3-butadiene)-polyethylene oxide diblock copolymer (IUPAC name: poly(but-2-ene-1,4-diyl)-block-polyoxyethylene) and water, and the rheological behavior of the solution. The degree of polymerization of the polybutadiene and polyethylene oxide blocks is 37 and 45, respectively. The diblock copolymer concentration was limited to be $\leq$ 2.5 wt% to avoid phase separation. Small X-ray scattering revealed that the diblock copolymer self-assembles in worm-like micelles with a diameter of $\sim$ 12 nm. This system does not closely follow the rheological behavior of worm-like micelle solutions made of typical surfactants. The system steadily shear thins reaching very low viscosity values at large shear rates, however there are not shear-thickening peaks. In thixotropic loops, the micellar solution does not present hysteresis. The viscoelastic spectra do not follow the Maxwell model at low and intermediate frequencies. This uncommon behavior for a worm-like micellar system is explained by the slow dynamics of the self-assembly. The extremely high hydrophobicity of the polybutadiene block does not allow any micellar rearrangement

1 Introduction

Amphiphiles contain two or more chemically dissimilar segments that are covalently joined. The incompatibility between these molecular segments leads to local segregation and to the formation of self-assembled structures. This propensity is clear in solution, where the solvent could be selective: good for one molecular segment but poor for the other. Typical amphiphiles are surfactants, lipids, and amphiphilic diblock copolymers. Diblock copolymers are important materials for creating self-assembled structures. Segregation of the different polymer blocks yields molecular-scale aggregates of nanometric size with great potential applications in nanostructured plastics [1]. In solution as nano- to micro-sized carriers of active compounds, *e.g.* pharmaceuticals [2], for the controlled release of encapsulated compounds. These are just a couple among numerous applications [3,4].

Diblock copolymers form aggregates or supramolecular structures in solution, whose morphology can be tuned (going from spheres, cylinders, worms, vesicles, bilayers, etc.) by varying the chemical nature of the blocks, their molecular weight, or their ratio. The preferred geometry is fixed by the spontaneous curvature determined by the most effective packing of the assembled aggregates. The spontaneous curvature optimizes the system energetically, but it does not account for the effects of entropy that can stabilize some structures and defects. At low concentration below the critical micelle concentration (CMC), which is quite low in diblock copolymers, entropy favors a uniform dissolution of the amphiphile in the solvent; aggregation is negligible. Above the CMC, interaction dominates and entropy effects are reduced. Consequently the number of aggregates, usually of a spherical form, sharply increases. Cylindrical micelles are formed by amphiphiles with moderate spontaneous curvature, lower than spherical micelles but larger than vesicles or bilayers. In cylindrical micelles, energy is optimized when the curvature is uniform everywhere, forming long linear structures (worm-like micelles, WLMs). However, entropy introduces in the system a degree of randomness through bending of cylindrical micelles, which adds conformational entropy in a manner similar to the configurational entropy of polymeric chains, and through topological defects, in the form of end-caps and/or branch junction points. These two defects are introduced by the formation of regions with differing local curvatures, but incurring in different energetic penalties. The overall entropic gain associated with end-caps is greater than that of branch points. Although the appearance of topological defects introduces an entropy gain, the

[a] e-mail: rolandoc@fisica.unam.mx

type of defect that dominates the system is set by the amphiphile spontaneous curvature. If the scission energy of a WLM (the energy required to creating two end-caps from an infinite cylinder) is large enough, then the semiflexible linear micelles may become very long and entangled, at a relatively low total volume fraction of surfactant. End-caps increase entropy by increasing the number of micelles in a given system. Thus, lowering the scission energy shortens the total contour length of the linear micelles. On the other hand, branch junction points increase the number of possible configurations, enabling percolation, and the formation of extended micellar networks, which lead to a multi-connected rather than an entangled network of cylindrical micelles. A review about junctions and end-caps can be found elsewhere [5]. In diblock copolymers recent advances have shown that stability of different morphologies can be tuned by varying the solvent composition [6,7], because of the free-energy contribution from the interfacial tension between the solvent and the insoluble block. Therefore, a complex interplay between molecular geometry and amphiphilic character of the diblock copolymer determines the organization of supramolecular structures. This interplay leads to take into account the micellar core that could be partially swollen by poor solvent, the surface free energy per chain associated to the core-corona interface, and the structure of the corona; the latter is determined from a balance among the elastic stretching of their constitutive blocks, and the repulsive interaction among their monomers.

In common surfactant solutions forming WLMs, above the overlap concentration (C^*) that defines the boundary between dilute and semidilute regimes, micelles are entangled. WLM solutions in most of the cases present a Maxwellian behavior at low and intermediate frequencies, non-linear rheological behavior with a plateau in the shear stress (σ) *vs.* shear rate ($\dot{\gamma}$) flow curve, and shear banding [8,9]. When an imposed shear rate exceeds a characteristic structural relaxation time, an inhomogeneous state is reached in which shear bands of fluids with different viscosities coexist separated along the gradient direction [10]; imposed shear stress can also produce bands in the vorticity direction. Below the overlap concentration, but above the CMC, the long micelles are on average not overlapping. Here in spite of the low surfactant concentration, micellar fluids can present shear thickening and rheopexy. Although specific features change from one system to another, dilute WLM solutions have characteristics in common. In most of them, when the shear rate increases steadily, curves of apparent viscosity (η) *vs.* $\dot{\gamma}$ present shear thickening above a critical shear rate ($\dot{\gamma}_c$). After reaching a maximum, where apparent viscosity increased by a factor of 2–50, the system shear thins. Before $\dot{\gamma}_c$ the system is Newtonian or slightly thinning [11–13]. However, after a sudden application of a constant shear rate larger than $\dot{\gamma}_c$, there is usually an induction period ($\tau_{\rm ind}$) where shear stress increases sharply up to a steady-flow plateau; $\tau_{\rm ind} \sim 1/\dot{\gamma}_c$ [13,14]. Small-angle neutron scattering (SANS) studies strongly suggest that the increase in viscosity observed above $\dot{\gamma}_c$ is associated with a shear-induced growth of the micellar aggregates [15].

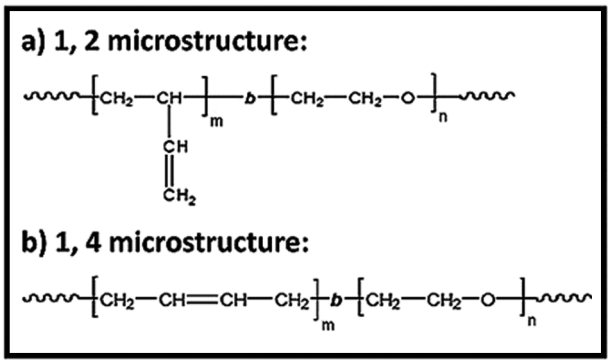

Fig. 1. Diblock copolymers of the type polybutadiene-polyethylene oxide showing two different polybutadiene microstructures: a) P(1,2)B; source name: 1,2-poly(1,3-butadiene); IUPAC name: poly 1-vinylethylene. b) P(1,4)B; source name: 1,4 poly(1,3-butadiene); IUPAC name: poly(but-2-ene-1,4-diyl).

In addition, SANS scattering data under shear [16] have established a correlation between flow and structure. In the thickening region, SANS patterns were interpreted as the superposition of two coexisting states, one viscoelastic entangled sheared network (shear-induced structures) and one still purely viscous containing unstructured aggregates; at larger $\dot{\gamma}$, the former state dominates and its increasing orientation results in shear thinning [13,17–20].

The most extensively studied diblock copolymers of the type polybutadiene-polyethylene oxide in water solution are those rich in the 1, 2-microstructure (IUPAC name: poly1-vinylethylene) [21–26]; see fig. 1. They will be referred to as P(1,2)B-PEO from now on (IUPAC name: poly1-vinylethylene-block-polyoxyethylene). Morphology of the supramolecular structures of these copolymers depends on the weight fraction ($w_{\rm PEO}$) of polyethylene oxide (PEO) in the copolymer, which is related to the hydrophilic block length, and on the degree of polymerization of the hydrophobic block, P(1,2)B. Aggregation in dilute aqueous solutions leads to spherical micelles approximately at $w_{\rm PEO} > 0.6$, WLMs approximately in the range of $0.47 < w_{\rm PEO} < 0.59$, and bilayers at $w_{\rm PEO} < 0.47$ [23,27]. A well-studied series is the symmetric P(1,2)B-PEO with a roughly equal number of hydrophobic and hydrophylic groups ($w_{\rm PEO} \approx 0.5$) [23, 27]. Symmetric P(1,2)B-PEO forms WLMs in aqueous solutions at concentration less than 5 wt%. At modest concentrations, *ca.* 5 to 10 wt%, a nematic phase of linear cylindrical micelles is formed, and above 10 wt% hexagonal structures are found. The tendency to form lamellar and hexagonal phases decreases with the increase of P(1,2)B-PEO asymmetry. One important difference between small non-ionic surfactants and diblock copolymers dispersed in a polar solvent, such as water, is the value of the CMC. For the former ones the CMC is not too low; molecular exchange and equilibration are relatively rapid. On the contrary for the latter ones, molecular exchange should be extremely slow due to the very small CMC ($\leq 10^{-6}$ M) that decreases as temperature increases; presence of free chains in solution is practically negligible. This impediment of micellar rearrangement has its origin on

the extremely high hydrophobicity of the P(1,2)B block. Therefore, observed aggregates are not necessarily at equilibrium. In many diblock copolymers micellar systems the core-forming block is vitrified, although this is not the case for P(1,2)B cores; glass temperatures $< 0\,^{\circ}$C [28]. In particular for the case of WLMs of P(1,2)B-PEO, no detectable exchange of unimers between aggregates and the solution has been detected by using a combination of deuterium labeling and time-resolved SANS techniques [29]. Direct evidence from cryogenic transmission electron microscopy has shown the slow micelle dynamics; there is no perceptible exchange of macromolecules among aggregates, and equilibrium is never achieved [24]. This failure to globally equilibrate has profound consequences on the distribution of morphologies that are kinetically trapped in these dispersions. These effects are evident even at molecular weights of just 2000 Da.

There are not many rheological studies on P(1,2)B-PEO diblock copolymers in water solution, particularly when they self-assemble in WLMs. P(1,2)B-PEO with a molecular weight of 4.9 kg/mol and their cross-linked versions have been studied by Y.Y. Won *et al.* [22] Förster *et al.* [30] found that shear thinning and orientation occurs for $\tau_{\rm dis}\dot{\gamma} \gg 1$ in WLMs of P(1,2)B-PEO ($m = 43$, $n = 59$, and $m = 27$, $n = 51$); $\tau_{\rm dis}$ is the disentanglement time. Here, the system shear thins as $\eta = \eta_{S0}e^{-aS}$, where S is the order parameter $S = \langle(3\cos^2\delta - 1)/2\rangle$, $\langle\delta\rangle$ is the mean deviation angle with respect to the flow direction, and α is a parameter of the exponential shell density profile; concentration and micellar thickness enter only in the prefactor. Lonetti *et al.* [31] also studied the microscopic mechanism behind the strong shear-thinning behavior of WLMs made of P(1,2)B-PEO in water ($m = 48$, $n = 54$)[1]. Shear thinning is due to critical slowing down of the orientational Brownian diffusion, as a result of the vicinity of the isotropic-nematic spinodal. The bimodal and spinodal curves for the isotropic-nematic phase transitions were determined in the $\dot{\gamma}$-C plane. In a certain shear rate range, shear thinning is so strong than shear banding occurs.

The aim of this study is twofold: First, to determine the structure of the self-assembled aggregates made of 1,4 poly(1,3-butadiene)-polyethylene oxide diblock copolymer (from now on: P(1,4)B-PEO; IUPAC name: poly(but-2-ene-1,4-diyl)-block-polyoxyethylene) in water; unknown as far as we know. Second, to determine the rheological behavior of the aqueous solution of this diblock copolymer. The solution concentration (C in P(1,4)B-PEO wt%) were limited to $C \leq 2.5$ wt % to avoid phase separation. The hydrophobic block, P(1,4)B is rich in 1,4 microstructure, see fig. 1. The degree of polymerization of the P(1,4)B and PEO blocks used here are $m = 37$ and $n = 45$, respectively. This system is similar the those made with P(1,2)B-PEO [24], which self-assembles in spheres, cylinders or bilayers, when the polymer blocks have a degree of polymerization ($m = 46$, and $n = 35$, 39 42, 44, 56) relatively close to those of the blocks used in this work. The results of the paper are divided in two parts. In the first one, the experiments for determining the morphology of the self-assembled structures are presented. The second part is devoted to present the rheological behavior of the diblock copolymer solution.

[1] This group does not clearly state what type of polymer microstructure they investigate. It seems to be P(1,2)B-PEO due to their synthetic references and their comparisons with the Bates' group results.

2 Experimental section

Materials and sample preparation. Poly(but-2-ene-1,4-diyl)-block-poly(oxyethylene) block copolymer ((P(1,4)B-PEO) = –[CH_2–CH=CH–CH_2]$_m$–b–[CH_2CH_2–O]$_n$– with $m = 37$, $n = 45$, $M_w = 4000$ g/mol) was purchased from Polymer Source (Canada); it was used as received. The polybutene block is rich in 1, 4 microstructure > 93 wt% as determined by H-NMR spectroscopy. Data given by the manufacturer: 2000-b-2000, $M_w/M_n = 1.08$, cis: 68 wt%, trans: 27 wt%, and 1, 2 microstructure ~ 5 wt%. A stock of P(1,4)B-PEO water solution was prepared by weight, and it was stirred for 14 days at 40 °C prior to be used. No phase separation was observed up to $C = 2.5$ wt%. Water was Milli-Q water (nanopure-UV, USA; resistivity ~ 18.3 MOhm cm).

Light Scattering. The experimental set up for dynamic light scattering (DLS) is a homemade apparatus. Laser light (Ar-ion, Spectra Physics, CA) illuminates the sample in a thermal bath at $T = 20 \pm 0.2\,^{\circ}$C. Dispersed light is detected with a THORN EMI photomultiplier (THOM-EMI, U.K.) coupled to an ALV preamplifier, and to an ALV-5000/E multiple tau digital correlator (ALV Langen, Germany) for getting the intensity autocorrelation function, $g^{(2)}(q,t)$; q is the magnitude of the scattering vector. The measured intensity autocorrelation function was converted into the electric field autocorrelation function, $g^{(1)}(q,t)$, by using the Siegert equation. Relaxation times were obtained using CONTIN-ALV software. DLS experiments were performed on micellar solutions at several angles. A regularized inverse transformation algorithm, incorporated in the ALV/5000/E program, was used to obtaining the relaxation time distribution peaks from the $g^{(1)}(q,t)$ functions, as well as the relaxation times ($\tau_{\rm rel}$) or decay rates, $\Gamma = D_T q^2 = \tau_{\rm rel}^{-1}$; D_T is the diffusion coefficient that can be obtained from the slope of Γ *versus* q^2. Static light scattering (SLS) experiments at low angles were performed with a goniometer-based 3D light scattering instrument (LS-instruments AG, Fribourg, Switzerland) provided with a multitau digital correlator and a He-Ne laser.

Small angle X-ray Scattering (SAXS). The experimental setup is a Rigaku (Japan) apparatus provided with a MicroMax-002 source with CMF optic, with three pinhole collimation optics for SAXS and WAXS placed in a three-meter long evacuated camera (0.133 Pa), and with an integrated 2D multi-wire proportional counter; $\lambda = 1.54$ Å and the nominal measurement range for q is: $0.006 < q < 0.48$ Å^{-1}. Measurements were taken at room temperature

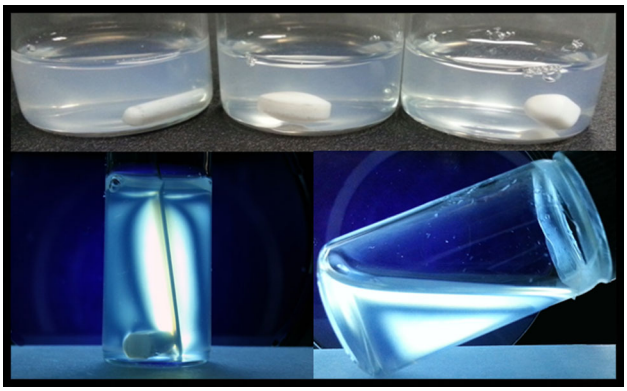

Fig. 2. Water solutions of P(1,4)B-PEO. Upper panels: Dilute solutions scatter light: From left to right $C = 2$ w%, 1 w%, and 0.7 w%. Lower panels: Solutions between cross polarizers under shearing: From left to right: A spatula is slowly dipped into the fluid, $C = 2.5$ w%, the sample is gently swiveled, $C = 1.7$ w%.

on samples of $\sim 70\,\mu$L at $C = 1$ and 2 wt% SAXS data analysis was performed with PCG Software (GIFT and DECON).

Rheology. Shear flow curves and viscoelastic spectra were measured in a Bohlin Gemini HRnano rheometer (Malvern Instruments, UK). All rheometric measurements were performed using a cone-plate geometry (4°-40 mm) with temperature control; all measurements were done at 20 °C.

3 Results and discussion

3.1 Structure of the aggregates

Determining the structure of the aggregates in a system is critical for understanding its rheological behavior. In the system of interest here, there is some kind of aggregation that is revealed by the scattering of light in dilute solutions. In these aggregates, the highly insoluble P(1,4)B block is surely hidden from water. At rest, dilute solutions are not birefringent. However, birefringence appears when they are sheared; see fig. 2.

Dynamic light scattering. The diblock copolymer solutions are not transparent. They look turbid even at very low concentrations (fig. 2), as if they contain large aggregates that scatter light. Figure 3a presents a typical example of an intensity autocorrelation function as a function of the delay time for the P(1,4)B-PEO/water system. Exponential fitting reveals that this function is by far not a single-exponential decay function. The relaxation time distribution, as calculated by CONTIN from the autocorrelation function, reveals that the objects that scatter light present a large degree of polydispersity (fig. 3a). Figure 3b presents Γ *vs.* q^2 for the mode corresponding to the peaks in the relaxation time distributions for different polymer concentrations ($C = 0.3$, 0.7, 1.0, and 2.0 wt%). The experimental points are noisy, and only for lower concentrations ($C = 0.3$ wt% and $C = 0.7$ wt%) the intercept is relatively close to zero. However in all the cases, the correlation coefficients for the linear fitting are between 0.93 and 0.97. Therefore, this is a diffusive mode and $\Gamma = 1/\tau = D_T q^2$. In the inset of fig. 3b, we present the diffusion coefficients obtained from the slope of Γ *vs.* q^2 at different concentrations. For $C = 0.3$, 0.7, 1.0, and 2.0 wt%, $D_T = 4.06 \times 10^{-12}$, 5.57×10^{-12}, 6.07×10^{-12}, and $11.63 \times 10^{-12}\,\mathrm{m^2\,s^{-1}}$, respectively. The impediment of micellar rearrangement observed in WLMs discussed in the Introduction could cause a large contour length polydispersity, and consequently the noise in the Γ *vs.* q^2 curves. A large contour length polydispersity was also observed in a WLM system made of P(1,2)B-PEO (see footnote[1]) with $m = 48$, $n = 54$ [7]. At low concentrations in small surfactants, previous studies have reported that the intensity time correlation function becomes bimodal as the surfactant concentration increases [32,33]. Because the dynamic structure factor, $S(q,t)$, exhibits a fast and slow mode (*i.e.* a double-exponential form) for wave vectors, q, such that $q\xi \ll 1$, where ξ is the WLM solution correlation length [32]. The fast mode is diffusive, *i.e.*, $\tau \sim q^{-2}$,

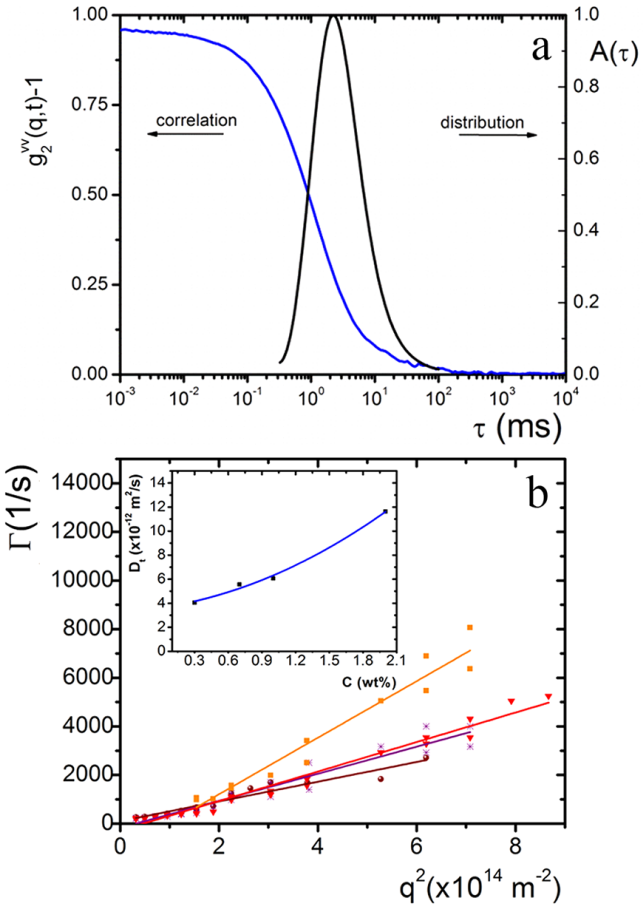

Fig. 3. Dynamic light scattering results for the P(1,4)B-PEO/water system. a) Typical intensity autocorrelation function (blue line) and relaxation time distribution $A(\tau)$ (CONTIN plot, black line), both as a function of delay time; $C = 0.7$ wt%, and $\theta = 45°$. b) Γ *vs.* q^2 for $C = 0.3$ •, 0.7 ∗, 1.0 ▼, and 2.0 ■, all in wt%; inset: D_T *vs.* C.

where $\tau = 1/Dq^2$ and $D = k_BT/6\pi\eta_0\xi$; here, T is absolute temperature, η_0 is the solvent viscosity, and k_B is the Boltzmann constant. This feature helps to discriminate between two concentration regimes defining the overlap concentration. At very low surfactant concentrations in the dilute regime, $C < C^*$, the fluid is made essentially of WLMs that are relatively far apart, producing a fast mode due to the WLM diffusion. The micelle growth associated with the increase of the surfactant concentration should produce a decrease in the diffusivity of the WLMs, until a concentration around C^*; here, micelle overlapping and entangling commence. After this concentration the fast mode relaxation time exhibits a monotonic decrease, and consequently, diffusivity increases. At higher surfactant concentration, in the semidilute regime $C > C^*$, a slow mode is observed; it corresponds to structural relaxation of the network as a consequence of the WLM entangling. As concentration increases above C^*, the slow mode of very small amplitude begins to evolve; the slow mode relaxation always increases and becomes very prominent. These features common in small surfactants [13,33] are not observed here. In our case, there is no local minimum at C^* in the D_T *vs.* C graph (inset fig. 3b), although it was possible to estimate C^* (~ 0.6 wt%) with viscosity measurements; this will be presented below. An estimation of the fluctuation correlation length from the measured D_T at the lowest concentration gives $\xi = 52.6\,\text{nm}$. Usually ξ is larger than the radius of gyration.

Depolarized DLS experiments were performed for exploring the possibility of acquiring information about the size and shape of the scattering particles through the rotational diffusion. Although VH intensity autocorrelation functions were obtained at low angles to avoid overlap between modes, polydispersity did not allow us to get information. It was concluded from these experiments that they do not seem to be compatible with spherical aggregates in the solution.

SAXS and SLS. Figure 4 presents the X-ray scattering intensity at low angles, $I_s(q)$, *vs.* q for the water solution of P(1,4)B-PEO at 2.0 wt%; essentially the same curve is obtained for 1.0 wt% SLS results for low q values were also included in this figure. The inset (a) of fig. 4 presents the X-ray scattering intensities obtained by a 2-dimensional multi-wire proportional counter. The scattering is isotropic; this reveals that there are no orientational degrees of freedom in the fluid. In conventional evaluation methods of SAXS data, the cross-section scattering function ($I_c(q)$) for rods of length L and diameter d is computed with $I_s(q) = (\pi L/q)I_c(q)$, where $d \ll L$; here, $I_s(q)$ is the scattering function. The transformation into the real space is made through $p_c(r) = (1/2\pi)\int_0^\infty I_c(q)rqJ_0(qr)\mathrm{d}q$, but this can be very difficult because of the strong termination effect; $p_c(r)$ is the cross-section pair distance distribution function, and J_0 is the Bessel function of order zero. Alternatively, we used the indirect Fourier transformation (IFT) method to extract information from the experimental $I_s(q)$. This method allows the computation of $I_c(q)$ and $p_c(r)$ with only one mathematical operation from the experimental data. However, an estimate for the maximum cross-section dimension for the cylinder is needed; data of P(1,2)-PEO WLMs from literature were used. In this method, it is assumed that $p_c(r)$ can be described with a series of cubic B-splines with unknown expansion coefficients. These coefficients are determined by a weighted least-squares approximation to the experimental data, where a stabilization condition is added to avoid oscillations in the solutions. In this way, an approximation to the experimental data ($I_c^{\mathrm{IFT}}(q)$) and to $p_c^{\mathrm{IFT}}(r)$ are obtained. For details see refs. [34,35]. The deconvolution of the convolution square function, $\tilde{\rho}^2(r)$, can be developed, when the radial density function is described with a series of simple step-functions. When these functions are included in $p_c(r) = r\tilde{\rho}^2(r) = r\int_{-\infty}^{\infty}\rho(x)\rho(x-r)\mathrm{d}x$ a system of non-linear equations is obtained that can be solved with an iterative stabilized weighted least-squares procedure. This allows the computation of $p_c(r)$, that we will call $p_c^{\mathrm{conv}}(r)$, as well as the radial electron density profile $\rho_c(r)$. $I_c^{\mathrm{conv}}(q)$ can be recovered ($= 2\pi\int_0^\infty p_c(r)J_0(qr)/q\,\mathrm{d}r$) from $p_c^{\mathrm{conv}}(r)$, For details see refs. [34,36].

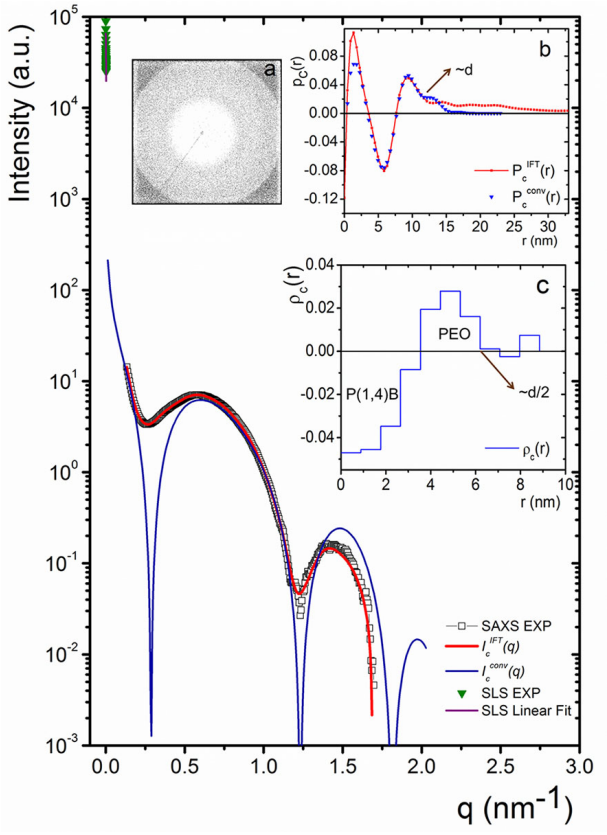

Fig. 4. X-ray scattering intensity at low angles *vs.* q for the solution of P(1,4)B-PEO in water. Experimental data (□) for SAXS, $C = 2$ wt%, Experimental data for SLS (▼), $I_c^{\mathrm{IFT}}(q)$ (red line) and $I_c^{\mathrm{conv}}(q)$ (blue line) both for cylinders. Insets: a) X-ray scattering intensities in a 2-dimensional multi-wire proportional counter. b) $p_c^{\mathrm{IFT}}(r)$in red and $p_c^{\mathrm{conv}}(r)$in blue. c) The radial electron density distribution *vs.* r.

In fig. 4 the resulting $I_c^{\mathrm{IFT}}(q)$ for cylindrical rods obtained by the IFT method (red continuous line) is included.

The fitting is very good taking into account the limited q-values where experimental points are available. Inset (b) of fig. 4 presents $p_c^{\mathrm{IFT}}(r)$ also obtained with the IFT method (red line). $p_c^{\mathrm{IFT}}(r)$ presents an oscillation that agrees with the fact that P(1,4)B-PEO forms WLMs that are not homogeneous. Surely, they have a hydrophobic core formed by the P(1,4)B block and a corona formed by hydrophilic PEO. $p_c^{\mathrm{IFT}}(r)$ shows a curvature change after the second peak [35] approximately at $\sim 11.2\,\mathrm{nm}$. In this inset $p_c^{\mathrm{conv}}(r)$ coming from the deconvolution method was also included; here, the curvature change after the second peak is also at $\sim 11.2\,\mathrm{nm}$. In the inset (c) of fig. 4, the radial electron density distribution $\rho_e(r)$ is presented. Clearly the micelle is made of two concentric cylinders of different electron density. The internal one that surely corresponds to the P(1,4)B block has a radius of $\sim 3.54\,\mathrm{nm}$, and the external one starts at this value and ends $\sim 6.2\,\mathrm{nm}$; after the signal oscillates around zero; thus, according to the electron density, the WLMs have a diameter $\sim 12.4\,\mathrm{nm}$. After a Hankel transformation on the obtained $p_c^{\mathrm{conv}}(r)$, the cross-section scattering function $I_c^{\mathrm{conv}}(q)$ can be recovered. This function was also included in fig. 4 (blue line). Given the limited available experimental points, we consider that the agreement with experimental data is good. It is important to note that the different structure of the P(1,4)B block apparently allows the core of P(1,4)B-PEO micelles to be more tightly packed. In contrast, the diameters of P(1,2)B-PEO WLMs are two or three times larger than those of P(1,4)B-PEO WLMs; both made with copolymers of approximately the same degree of polymerization [30,31].

As mentioned, SLS results were also included in fig. 4. This data shows a small curvature that is typical of polydisperse solutions; the scale of the figure does not allow to appreciating this feature. This effect surely comes from the micelle contour length polydispersity. However, we made a linear fitting of this data in fig. 4. The correlation coefficient of this fitting is 0.8. Then, scattering intensity roughly follows the q^{-1} dependence, which is typical of cylinders. Therefore, SAXS and SLS gives enough evidence to assure that the self-assembled structures in the water solutions of P(1,4)B-PEO are WLMs.

3.2 Rheological behavior

Flow curves and thixotropic loops. Figure 5 presents flow curves made by steadily increasing the level of applied shear stress (shear stress control), or by steadily increasing the level of applied shear rate (shear rate control) to micellar solutions at different concentrations; the sweeps were performed along four orders of magnitude in $\dot{\gamma}$. Shear stress increases in a non-linear way as the shear rate increases. Within the experimental error limits, shear rate control and shear stress control curves can be superimposed. This is not the behavior usually found in WLM solutions of common surfactants at low concentrations. There, a distinctive behavior occurs when the applied shear stress is steadily increasing under shear stress control: At some point in the flow curve the shear rate first

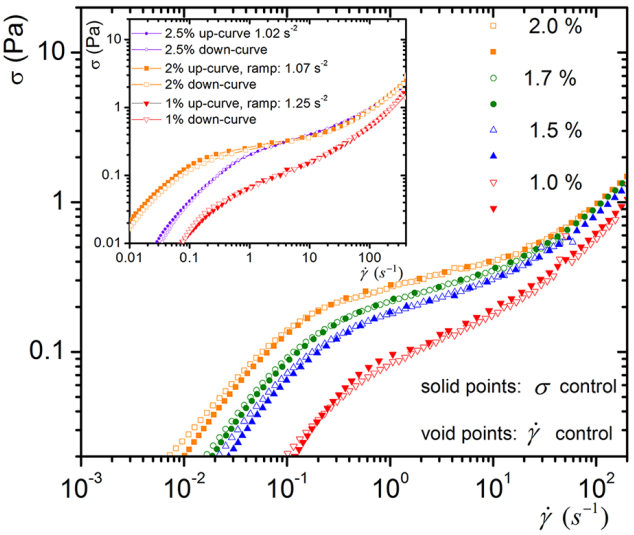

Fig. 5. Comparison between flow curve made under shear stress (solid points, rate of sweeping $\sim 0.006\,\mathrm{Pa\,s^{-1}}$) or shear rate control (void points, rate of sweeping $\sim 0.9\,\mathrm{s^{-2}}$) for micellar solutions of P(1,4)B-PEO at different concentrations. Inset: thixotropic loops for three copolymer concentrations; up-curves and down-curves are superimposed.

decreases, and then once again $\dot{\gamma}$ increases. On the contrary, under shear rate control, by steadily increasing the level of applied shear rate there is a jump in the shear stress. This behavior is presented by several surfactant solutions with WLMs; for examples see [13] and [19]. In fact, the σ *vs.* $\dot{\gamma}$ curves of fig. 5 present a plateau-like zone, which is typical of semidilute or concentrated micellar solutions ($C > C^*$), where shear banding is usually observed, suggesting at these concentrations we are above C^*. However, in normal surfactants at those concentration regimes, it is common that they present shear thickening previous to finding the plateau-like region in the up-shear curves (shear control) that is not observed in the up-stress curves (stress control). This behavior is not found here. The inset of fig. 5 presents examples of thixotropic loops for different concentrations. Here, the shear stress is first ramped up (up-curve) from $\sigma \sim 0$, to some maximum value and then it is ramped down (down-curve) at the same rate to $\sigma \sim 0$. Sweep times were of 1000 s for cycles between 2×10^{-4}-8.0 Pa that correspond to a rate of sweeping in shear rate of $1.25\,\mathrm{s^{-2}}$, $1.07\,\mathrm{s^{-2}}$, and $1.02\,\mathrm{s^{-2}}$ for $C = 1$, 2, and 2.5 wt%, respectively; these results did not change for slower rates of sweeping. Shear rate increases almost linearly as σ increases at low shear stress, but at larger shear stress, the shear rate increases in a non-linear way. Within the experimental error limits up-curves and down-curves can be superimposed, *i.e.*, the system does not present hysteresis that is common in many WLM systems [17,18].

Viscosity and flow curves. Figure 6a presents the apparent viscosity for the PB(1,4)-PEO/W system determined by steadily increasing the shear stress, at different copolymer

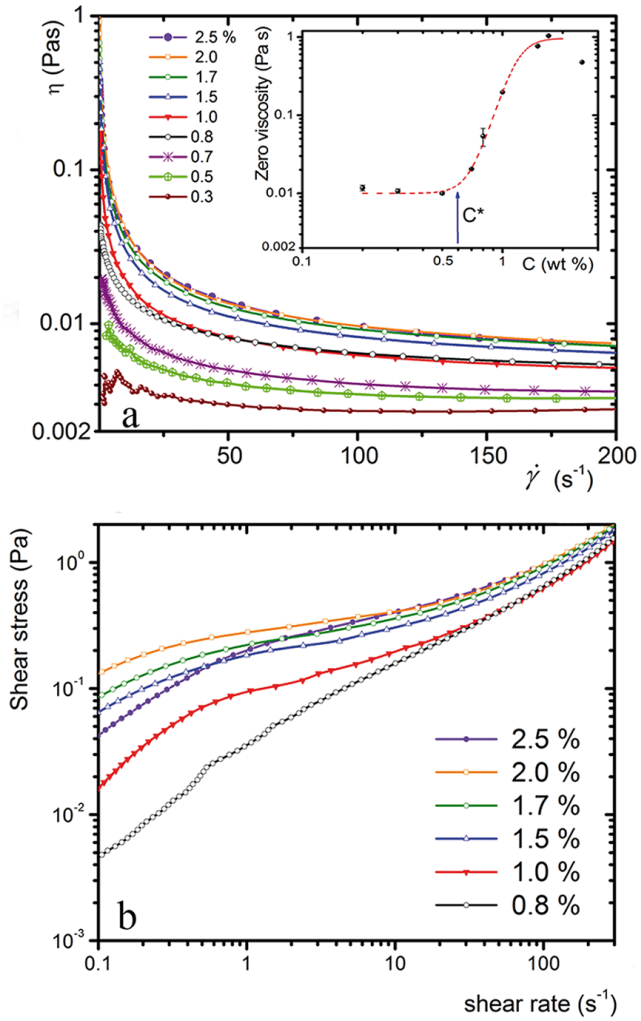

Fig. 6. a) Apparent viscosity of the P(1,4)B-PEO/water system at different concentrations determined with shear stress control. Inset: zero shear viscosity as a function of solution concentration. b) σ *vs.* $\dot{\gamma}$ flow curves which gave rise to the apparent viscosities presented in (a).

concentrations, $0.3 \leq C \leq 2.5$ wt%; the curves do not vary with sweeping time within the experimental error. $\eta(\dot{\gamma})$ is almost constant for $\dot{\gamma} > 50\,\mathrm{s}^{-1}$ at lowest concentration, $C = 0.3$ wt%; there $\eta(\dot{\gamma})$ is ~ 3 times larger than the solvent viscosity. In general, at larger concentrations, the viscosity curves moves upward in this diagram. Although, for $C = 2.5$ wt%, the viscosity curve is a little below than the viscosity curves for other solutions with lower concentration, particularly at low shear rates. The system steadily shear thins as $\dot{\gamma}$ increases, and very low viscosity values are reached at large shear rates ($\eta > 0.008\,\mathrm{Pa\,s}$). There are several mechanisms that could be responsible for the occurrence of strong shear thinning. One mechanism is related to breakage and recombination. Here, scission due to shearing forces and merging of worms through stressed entanglement points can lead to strong shear thinning [37]. Another possible mechanism for strong shear thinning is connected to the fact that WLM systems can undergo an isotropic-nematic phase transition [31]. In fact, the system studied here is close to an isotropic-nematic transition, *i.e.*, to the binodal line in the $\dot{\gamma}$-C plane. Rotational diffusion close to the phase diagram spinodal line is very slow (critical slowing down), so that a relatively strong alignment on applying shear flow occurs. Such a strong increase in the degree of alignment leads in turn to strong shear thinning. Then, rotational diffusion is constrained by entanglement and shear induces micelle orientation as shown by the relation $\eta \sim e^{-aS}$ [30]. The inset of fig. 6a presents $\log[\lim_{\dot{\gamma}\to 0}\eta(\dot{\gamma})]$ *vs.* $\log C$, where a change of behavior is clearly observed at ~ 0.6 wt%. Below this concentration, the interaction between micelles apparently is negligible as in the dilute regime; here viscosity is low and relatively close to the solvent viscosity. After this concentration micelles start to entangle, and viscosity increases drastically as in the semidilute regime. Therefore, the overlap concentration is $C^* \sim 0.6$ wt%.

Figure 6b presents the σ *vs.* $\dot{\gamma}$ flow curves that gave rise to some of the viscosity curves of fig. 6a for different concentrations; $0.8 < C < 2.5$ wt%. These curves exhibit a pronounced shear thinning particularly at the stress plateau region, which extends to lower shear rates and becomes flatter as the concentration increases from $1.0 \leq C \leq 2.0$. There is no plateau-like region below $C = 1$ wt%. The behavior of the flow shear curve corresponding to $C = 2.5$ wt% is peculiar. Approximately, it has the same viscosity at high shear rates as the other solutions above 1.5 wt%, and it is not significantly different at low shear rates. However, the stress plateau region is smaller. This behavior is similar what occurs in the isotropic-nematic phase transition as observed in the σ-$\dot{\gamma}$ plane. In many WLM systems by using a superposition procedure, it is possible to sum up all the flow behavior at many different concentrations and temperatures on one single master dynamic phase diagram [38,39]. In this diagram the stress plateau region decreases as we move upward below the coexistence dome, and no plateau is detected above the critical temperature. The flow shear curve for $C = 2.5$ wt% would seem to be around the critical temperature in this diagram. The diagram can be generated because solutions behave as Maxwellian fluids, and the elastic plateau modulus and the relaxation time are used for normalizing σ, and $\dot{\gamma}$. However, as we will see below, the system under study here does not behave as a Maxwellian fluid. Birefringence is a landmark for shear banding that was observed in this system (see fig. 2); the features of this behavior is under study and will be reported soon.

Viscoelastic spectra. In WLM solutions the shear modulus, $G(t)$, exhibits a significant time or frequency dependence. The latter is expressed through the complex modulus $G^*(\omega) = G'(\omega) + iG''(\omega)$; $G^*(\omega) = i\omega \int_0^\infty G(t)e^{-i\omega t}\,\mathrm{d}t$. The real part of the complex modulus is the storage, or elastic, modulus in phase with the applied shear strain. The imaginary part is the viscous, or loss, modulus in phase with $\dot{\gamma}$. Figure 7 presents the viscoelastic spectra of the micellar solution of P(1,4)B-PEO for different concentrations. In general, the solutions are more viscous at low frequencies. At larger frequencies, after a cross-

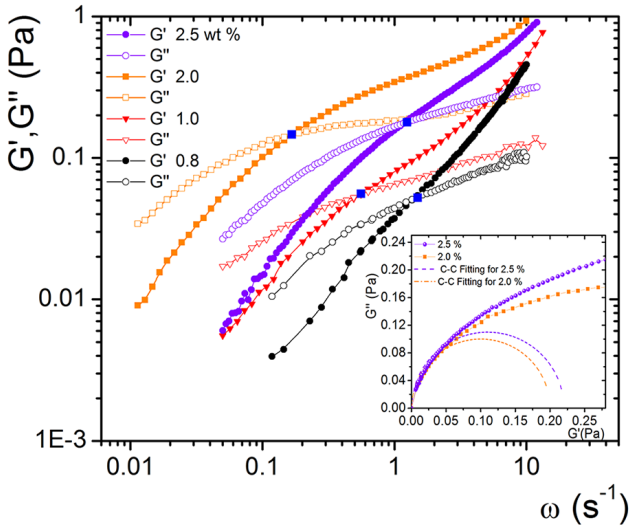

Fig. 7. The viscolelastic spectra for the P(1,4)B-PEO/water system at different concentrations. Inset: G' *vs.* G'' for $C = 2.0$ and 2.5 wt%, and fittings as in the Cole-Cole plots.

ing point, the solutions are more elastic. G_o, defined at the crossing point, (ω_o, G_o), increases as the concentration increases. The G_o values are quite low ($\sim$ 0.18 Pa at $C = 2.5$ wt%) for P(1,4)B-PEO solutions when compared with the G_o values for WLM solutions of common surfactants (1–1000 Pa), and of the same order of magnitude for similar diblock polymer WLMs made of P(1,2)B-PEO ($\sim$ 0.25 Pa) [40]. The crossover frequency, ω_0, decreases as the concentration increases, except for the case of $C = 2.5$ wt%. Inversely related, the relaxation time $\tau = \omega_o^{-1}$ increases as concentration increases until $C = 2$ wt% ($\tau \sim 6.8$ s); for $C = 2.5$ wt%, $\tau \sim 0.8$ s. $G'(\omega)$ and $G''(\omega)$ do not correspond to the elastic and viscous modulus of a Maxwellian fluid, which is the model followed by most of the WLM solutions at low and intermediate frequencies. The inset of fig. 7 presents a plot of G'' *vs.* G' for developing a Cole-Cole diagram for the case of the more concentrated solutions; there is no way to get a semicircular fitting that is a necessary condition for Maxwellian behavior. Above 2.5 wt%, the micellar solution presents a phase separation; the new phase is birefringent. This avoids getting viscoelastic spectra for more concentrated solutions. Since this system forms WLMs, this uncommon behavior could be explained because of the impediment of any micellar rearrangement, due to the extremely high hydrophobicity of the P(1,4)B block. Maxwellian behavior in WLMs is explained because local stress relaxes through a combination of reptation and/or breakage and recombination mechanisms [41]; the characteristic time of the latter is quite short with respect to the former. As a consequence $G(t) \sim \exp(-t/\tau_M)$ ensues for Maxwell fluids; τ_M is the Maxwell relaxation time, which is the geometric mean of both relaxation times [41]. This $G(t)$ does not describe the system under study. If $G^*(\omega)$ is calculated for $G(t) \sim \exp(-(t/\tau_R)^{1/4})$ that corresponds to the case of a polymer relaxing just through reptation, the fitting to the experimental $G'(\omega)$ and $G''(\omega)$ curves is not good. However, when $G(t) \sim \exp(-(t/\tau)^{1/2})$ is used, which corresponds to an intermediate case where the characteristic time, τ, considers reptation and for breakage/recombination of the same order of magnitude, the fitting is much better (not shown). Micelles do not break and reform as in Maxwell fluids, but they are not completely frozen as in the case of chemically bonded polymers. This agrees with the impediment of micellar rearrangement. At the higher frequencies that mechanical rheometry allowed us to make a measurement, the moduli ($|G^*|$) of the concentrated micellar solutions seems to follow a power law, $|G^*| \approx \omega^{5/9}$; here, micelles can be regarded as semiflexible chains. This could be indicative that at these frequencies, the stress apparently relaxes via an intramicellar processes dominated by the Rouse-Zimm modes.

4 Concluding remarks

It was found that the solution of 1,4 poly (1,3-butadiene)-polyethylene oxide in water self-assembles in worm-like micelles. The degree of polymerization of the P(1,4)B and PEO blocks is 37 and 45, respectively (cis: 68 wt%, trans: 27 wt%). On the average, the diameter of these cylindrical structures is $\sim$ 12 nm. This diameter is smaller than the diameter of other similar P(1,2)B-PEO diblock copolymers forming cylindrical micelles rich in 1, 2 microstructure ($\sim$ 28 nm) [30,31]. Approximately at concentrations larger than $C > 2.5$ wt%, the system phase separates where a birefringent phase and an isotropic phase coexist.

The rheological behavior of worm-like micelle solutions of typical surfactants is not entirely followed by this system [8,9,13,17–20,42]. At low concentration the solutions steadily shear thins as shear rate increases reaching very low viscosity values at large shear rates; there are not shear-thickening peaks. The boundary between dilute and semidilute regimes was estimated to be $\sim$ 0.6 wt%, according to the behavior of the zero shear viscosity. In thixotropic loops, up-shear and down-shear curves can be superimposed; the micellar solution does not present hysteresis as in common surfactants [13,19]. Flow curves determined with shear rate control and shear stress control can be superimposed. When sheared the micellar solutions present birefringence that is a clear landmark for gradient shear banding. Apparently these features make the system quite stable under flow. It is a good candidate to study the features of its gradient shear banding, which probably would be more stable than in other micellar systems with shear thickening [43]. The viscoelastic spectra do not follow the Maxwell model at low and intermediate frequencies, which is atypical in a worm-like micellar solution [8,38]. This uncommon behavior for a worm-like micelle system is explained by the slow dynamics of the self-assembly; there is an impediment of any micellar rearrangement, due to the extremely high hydrophobicity of the P(1,4)B block. This feature has been observed in similar diblock copolymers of the type P(1,2)B-PEO in other circumstances [24,29].

Funds from SEP-CONACYT (177679 and 152532) and DGAPA-UNAM (IN104911) are gratefully acknowledged. We acknowledge Dr. M. Carbajal-Tinoco for his help in the SAXS measurements, and to Drs. J. Delgado and E. Sarmiento for their critical discussions.

References

1. A.V. Ruzette, L. Leiber, Nat. Mater. **4**, 19 (2005).
2. S.J. Holder, N.A.J.M. Sommerdijk, Polym. Chem. **2**, 1018 (2011).
3. I.W. Hamley, Angew. Chem. Int. Ed. **42**, 1692 (2003).
4. T. Gadt, N.S. Leong, G. Cambridge, M.A. Winnik, I. Manners, Nat. Mater. **8**, 144 (2009).
5. N. Dan, S.A. Safran, Adv. Colloid Interface Sci. **123-126**, 323 (2006).
6. E.B. Zhulina, M. Adam, I. LaRue, S.S. Sheiko, M. Rubinstein, Macromolecules **38**, 5330 (2005).
7. B. Lonetti, A. Tsigkri, P.R. Lang, J. Setllbrink, L. Willner, J. Kohlbrecher, M.P. Lettinga, Macromolecules **44**, 3583 (2011).
8. J.F. Berret, *Rheology of Wormlike Micelles: Equilibrium Properties and Shear Banding Transitions*, in *Molecular Gels*, edited by R.G. Weiss, P. Terech (Springer, The Netherlands, 2006) p. 667.
9. C.A. Dreiss, Soft Matter **3**, 956 (2007).
10. P.D. Olmsted, Rheol. Acta **47**, 283 (2008).
11. C. Liu, D.J. Pine, Phys. Rev. Lett. **77**, 2121 (1996).
12. R. Gamez-Corrales, J.F. Berret, L.M. Walker, J. Oberdisse, Langmuir **15**, 6755 (1999).
13. D. Lopez-Diaz, E. Sarmiento-Gomez, C. Garza, R. Castillo, J. Colloid Interface Sci. **348**, 152 (2010).
14. H. Hu, S.Q. Wang, A.M. Jamieson, J. Rheol. **37**, 531 (1993).
15. R. Oda, V. Weber, P. Lindner, D.J. Pine, E. Mendes, F. Schosseler, Langmuir **16**, 4859 (2000).
16. J.F. Berret, R. Gámez-Corrales, J. Oberdisse, L.M. Walker, P. Lindner, Europhys. Lett. **41**, 677 (1998).
17. J. Delgado, R. Castillo, J. Colloid Interface Sci. **312**, 481 (2007).
18. J. Dehmoune, J.P. Decruppe, O. Greffier, H. Xu, P. Lindner, Langmuir **25**, 7271 (2009).
19. Y.T. Hu, P. Boltenhagen, D.J. Pine, J. Rheol. **42**, 1185 (1998).
20. Y.T. Hu, P. Boltenhagen, E. Matthys, D.J. Pine, J. Rheol. **42**, 1209 (1998).
21. Y.Y. Won, H.T. Davis, F.S. Bates, Science **283**, 960 (1999).
22. Y.Y. Won, K. Paso, H.T. Davis, F.S. Bates, J. Phys. Chem. B **105**, 8302 (2001).
23. S. Jain, F.S. Bates, Science **300**, 460 (2003).
24. S. Jain, F.S. Bates, Macromolecules **37**, 1511 (2004).
25. S. Jain, X. Gong, L.E. Scriven, F.S. Bates, Phys. Rev. Lett. **96**, 138304 (2004).
26. S. Forster, B. Berton, H.P. Hentze, E. Kramer, M. Antonietti, P. Linder, Macromolecules **34**, 4610 (2001).
27. Y.Y. Won, H.T. Davis, F.S. Bates, M. Agamalian, G.D. Wignall, J. Phys. Chem. B **104**, 7134 (2000).
28. N. Makhiyanov, E.V. Temnikova, Polym. Sci. A **52**, 1292 (2010).
29. Y.Y. Won, H.T. Davis, F.S. Bates, Macromolecules **36**, 953 (2003).
30. S. Förster, M. Konrad, P. Lindner, Phys. Rev. Lett. **94**, 17803 (2005).
31. B. Lonetti, J. Kohlbrecher, L. Willner, J.K.G. Dhont, M.P. Lettinga, J. Phys.: Condens. Matter **20**, 404207 (2008).
32. M. Adam, M. Delsanti, Macromolecules **18**, 1760 (1985).
33. S. Amin, T.W. Kermes, R.M. van Zanten, S.J. Dees, J.H. van Zanten, Langmuir **17**, 8255 (2001).
34. O. Glatter, *Fourier Transformation and Deconvolution*, in *Neutrons, X-ray and Light: Scattering Methods Applied to Soft Condensed Matter*, edited by P. Linder, Th. Zemb (North-Holland, Amsterdam, 2002).
35. O. Glatter, J. App. Crystallogr. **13**, 577 (1980).
36. O. Glatter, J. App. Crystallogr. **14**, 101 (1981).
37. W.J. Briels, P. Mulder, W.K. den Otter, J. Phys.: Condens. Matter **16**, S3965 (2004).
38. J.F. Berret, F. Porte, J.P. Decruppe, Phys. Rev. E **55**, 1668 (1997).
39. D. Lopez-Diaz, R. Castillo, J. Phys. Chem. B **114**, 8917 (2010).
40. Y.Y. Won, A.K. Brannan, H.T. Davis, F.S. Bates, J. Phys. Chem. B **106**, 3354 (2002).
41. M.E. Cates, Macromolecules **20**, 2289 (1987).
42. E. Cappelaere, J.F. Berret, J.P. Decruppe, R. Cressely, P. Lindner, Phys. Rev. E **56**, 1869 (1997).
43. J. Delgado, H. Kriegs, R. Castillo, J. Phys. Chem. B **113**, 15485 (2009).